A Silicon-Based Heterojunction Integrated with a Molecular Excited State in a Water-Splitting Tandem Cell

Journal:	*Journal of the American Chemical Society*
Manuscript ID	ja-2019-04238b
Manuscript Type:	Article
Date Submitted by the Author:	18-Apr-2019
Complete List of Authors:	Shan, Bing; University of North Carolina at Chapel Hill, Chemistry Brennaman, M. Kyle; University of North Carolina at Chapel Hill, Chemistry Ludovic , Troian-Gautier; University of North Carolina at Chapel Hill, Chemistry Liu, Yanming; School of Environmental Science and Technology, Dalian University of Technology, Nayak, Animesh; University of North Carolina at Chapel Hill, Chemistry Klug, Christina; Pacific Northwest National Laboratory, Physical Sciences Division Li, Ting-Ting; Ningbo University, Bullock, R. Morris; Pacific Northwest National Laboratory, Center for Molecular Electrocatalysis Meyer, Thomas; University of North Carolina, Chemistry

A Silicon-Based Heterojunction Integrated with a Molecular Excited State in a Water-Splitting Tandem Cell

Bing Shan[1], M. Kyle Brennaman[1], Ludovic Troian-Gautier[1], Yanming Liu[2], Animesh Nayak[1], Christina M. Klug[3], Ting-ting Li[4], R. Morris Bullock[3], Thomas J. Meyer[1]*

[1] Department of Chemistry, University of North Carolina at Chapel Hill, Chapel Hill, NC 27599, USA.

[2] Key Laboratory of Industrial Ecology and Environmental Engineering, Dalian University of Technology, Dalian 116024, China.

[3] Center for Molecular Electrocatalysis, Pacific Northwest National Laboratory, P.O. Box 999, K2-12, Richland, WA 99352, USA.

[4] Research Center of Applied Solid State Chemistry, Ningbo University, Ningbo 315211, China.

*E-mail: tjmeyer@unc.edu

ABSTRACT

Semiconductor-based photocathodes with high light-absorption capability are of interest in the production of solar fuels, but many of them are limited by low efficiencies due to rapid interfacial back electron transfer. We demonstrate here that a nanowire-structured p-type Si (p-Si) electrode, surface-modified with a perylene-diimide derivative (PDI'), can undergo photo-reduction of a surface-bound, water reduction catalyst towards efficient H_2 evolution under a low applied bias. At the electrode interface, the PDI' layer converts green light into high-energy holes at its excited state for extraction of photogenerated electrons at the photoexcited p-Si. The photogenerated electrons at the reduced PDI' are subsequently transferred to a surface-bound, molecular H_2-evolution catalyst. Involvement of the photoexcited PDI' enables effective redox separation between the electrons at the reduced catalyst and the holes at the valence band of p-Si. The heterojunction photocathode was used in a tandem cell by coupling with a dye-sensitized photoanode for solar-driven water splitting into H_2 and O_2.

INTRODUCTION

Solar-fuels provide an alternative to fossil fuels for powering the world's energy needs. In one approach, photoelectrochemical cells (PECs) are used to split water into O_2 and H_2, or to prepare a reduced form of carbon [1, 2]. In a single-junction, water-splitting PEC, the light absorber must have a sufficient bandgap to cover the energy losses in the device-operating voltages and the overpotentials for H_2 and O_2 evolution [3, 4]. Given the Shockley-Queisser limit [5], solar-conversion efficiencies of typical single-junction PECs are low due to thermodynamic constraints from the light absorbers. To overcome this limitation, tandem PECs, with more than one more light absorber, can be used to enhance efficiencies. In multi-photon absorption systems, analogous to the Z-scheme of natural photosynthesis, different parts of the solar spectrum are used to generate photovoltages needed to split water [6-13]. With photovoltage constraints met, the operating photocurrents for oxidation and reduction at the electrodes determine cell efficiencies. Compared to photoanodes for water oxidation, where significant progress has been made, photocathodes for water reduction have been far less efficient [14, 15]. Improving the overall efficiencies of tandem PECs for water splitting hinges on identifying high-performance, water-reduction photocathodes.

In water-splitting PECs, p-type Si (p-Si) has been used routinely as a photocathode material, because of its low cost, optimal band structure and crystallinity [16-23]. Water reduction at p-Si photocathodes is energetically feasible, but the rate of H_2 evolution is not competitive with back electron transfer at the photoexcited p-Si with a small band bending where reasonable photovoltage and photocurrent could be realized. Efficiency improvement depends on surface modification of p-Si to allow for efficient charge separation following photoexcitation. In the 1980's, Wrighton et al. reported enhanced interfacial charge separation at p-Si photocathodes by surface-modification with a methyl viologen-based polymer as a redox mediator [24, 25]. Addition of the mediator enabled efficient electron transfer to the electrode, but with a loss of driving force for activation of a H_2 evolution catalyst. A challenge in this area is to find a mediator with an appropriate redox potential for delivering electrons from the photoexcited p-Si to the catalyst.

We describe here a new water-splitting, tandem PEC with a nanostructured p-Si photocathode that is modified by addition of a perylene-diimide derivative (PDI') and a nickel-based molecular H_2 evolution catalyst (NiCt) [26-28]. The photocathode utilizes the highly electron-deficient PDI' excited state [29] as an electron transfer mediator that forms a one-electron reduced shuttle for effective activation of the catalyst. We also demonstrate that integration of the modified p-Si photocathode with a dye-sensitized photoanode in a tandem configuration enables relatively efficient overall water splitting into H_2 and O_2.

RESULTS AND DISCUSSION

The Si-based heterojunction with the structure shown in Figure 1a was synthesized from a planar, boron-doped p-Si(100) wafer. The wafer surface was etched into nanowire arrays with an average length of ~18 μm based on a reported method [30-32]. The p-Si nanowire electrode was subsequently modified by physical vapor deposition of a thin Ti layer (~ 10 nm), followed by atomic layer deposition (ALD) of a TiO_2 layer (~ 3.0 nm). The structure of the resulting p-Si|Ti|TiO_2 electrode is shown in the scanning electron microscope (SEM) images in Figure 1b. The TiO_2 layer deposited by ALD was added to protect the p-Si electrode from photodegradation. [33] It is also used as a bridging layer for binding the phosphonic acid anchoring groups at a molecular assembly [34]. As illustrated in

Figure 1a, the final photocathode structure has the molecular assembly consisting of PDI' and the NiCt catalyst $([Ni(P_2^{Ph}N_2^{C_6H_4CH_2PO_3H_2})_2]^{2+}$ [28] with the surface coverages listed in Table S1. In the assembly, the two molecules are covalently connected by a Zr^{IV}-phosphonate bridge [35, 36]. The synthetic procedure for preparing the photocathode is summarized in Figure S1.

Mott-Schottky analysis (Figure 1c,d) illustrates the capacitance-voltage (C-V) characteristics of the photocathodes with and without the molecular assemblies. Flat-band potentials were determined from linear fits of the depletion region (Figure 1c) [37] for the photocathodes in the dark. The resulting flat-band potentials (~ 0.13 V – 0.20 V vs NHE) are essentially invariant for p-Si|Ti|TiO_2 with and without the molecular assemblies. At a high frequency (1.0 kHz) of the applied alternating-current (AC) signal, the measured capacitance in the inversion region is minimized, because of the much slower change in electron density at the space-charge layer relative to the rapid AC signal [37, 38]. When illuminated (Air Mass 1.5 Global spectrum (AM 1.5 G), 100 mW cm^{-2}), the photocathodes exhibit significantly modified C-V characteristics, Figure 1d. The data for p-Si|Ti|TiO_2 in Figure 1d shows a transition from depletion to inversion at ~ 0.42 V vs NHE. Light illumination increases the measured capacitance in the inversion region. As observed elsewhere [37, 38], charge recombination within the inversion layer is usually significantly reduced, allowing for redox separation at the electrode-solution interface.

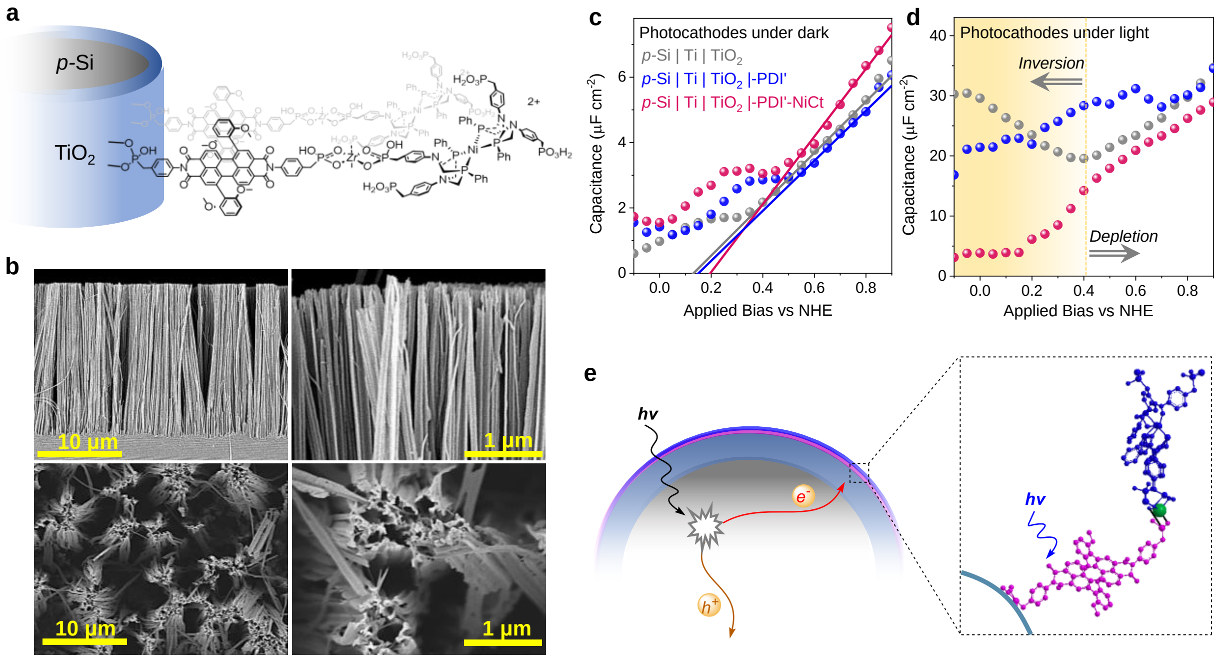

Figure 1. **a**, Structure of the photocathode assembly, -PDI'-NiCt, on the surface of p-Si|Ti|TiO_2. **b**, Scanning electron microscope (SEM) images for p-Si|Ti|TiO_2. **c**, Capacitance-voltage (C-V) curves recorded for p-Si|Ti|TiO_2 (grey), p-Si|Ti|TiO_2|-PDI' (blue) and p-Si|Ti|TiO_2|-PDI'-NiCt (red) in the dark. The solid lines are linear fits in the depletion region for estimating the flat-band potentials. **d**, C-V curves recorded for the photocathodes under illumination (AM 1.5 G), with the same color designations as in **c**. **e**, Schematic side view of p-Si|Ti|TiO_2|-PDI'-NiCt under illumination with the arrows representing light excitation (black and blue arrows) and electron-hole separation (red and brown arrows).

The photocathode p-Si|Ti|TiO_2|-PDI' exhibits C-V characteristics that are similar to p-Si|Ti|TiO_2. However, for p-Si|Ti|TiO_2 modified with the assembly (PDI'-NiCt) under illumination, the capacitance decreases sharply as the inversion region develops, which arises from water reduction leading to large current flow. As illustrated in Figure 1e, in the inversion region, the photocathode p-Si|Ti|TiO_2|-PDI'-NiCt captures incident photons and converts them into electron-hole pairs both at p-Si and at the assembly. The minority carriers (electrons) at photoexcited p-Si are transferred to the PDI' excited state and then to the NiCt catalyst toward water reduction to H_2.

To illustrate the effect of surface molecular modification on photoelectrocatalytic performances, linear sweep voltammetry (LSV) measurements were conducted for the photocathodes in a three-electrode cell with a Pt mesh as the counter electrode and a Ag/AgCl as the reference electrode in pH 4.5 acetate buffer with 0.9 M $NaClO_4$ as the supporting electrolyte. The presence of surface-immobilized PDI' is shown in the LSV of n-Si|Ti|TiO_2|-PDI' with a redox feature of the PDI'^0/PDI'^- couple at ~ -0.64 V vs NHE which is close to the potential of PDI'^0/PDI'^- on nanocrystalline ITO electrodes [29], Table S2. On p-Si|Ti|TiO_2, the redox feature of PDI'^0/PDI'^- is minimized in the dark (solid blue curve in Figure 2a). Under illumination, p-Si|Ti|TiO_2|-PDI' responds with an increase in photocurrents under bias more negative than ~ -0.5 V vs NHE. The photocathode with the full assembly, p-Si|Ti|TiO_2|-PDI'-NiCt, generates enhanced photocurrents as the bias passes ~ -0.3 V vs NHE (red dashed curve in Figure 2a), due to efficient water reduction catalyzed by the photo-reduced NiCt.

Surface molecular modification improves the output characteristics of p-Si by changing the number and location of surface states in p-Si where Fermi level pinning applies [24, 25, 39, 40]. For p-Si, the maximum open-circuit photovoltage (V_{OC}) varies with the amount of band bending and barrier height of the surface states. From the data in Figure 2b, V_{OC} of p-Si|Ti|TiO_2 under illumination (AM 1.5 G, 100 mW cm^{-2}) is ~ 0.32 V which is increased by ~ 0.21 V upon surface derivation with PDI'. The increase in V_{OC} originates from the electronic coupling between the PDI' excited state (PDI'*) and the photoexcited p-Si with changes in the electrode surface states. Subsequent addition of the NiCt layer on p-Si|Ti|TiO_2|-PDI' plays a small role with a decrease in V_{OC} of only ~ 0.04 V (red line in Figure 2b).

The energy-band diagram for p-Si|Ti|TiO_2|-NiCt in Figure 2c shows that the minority carriers (electrons) at photoexcited p-Si pass directly from the conduction band edge through the tunneling layers (Ti|TiO_2) to the NiCt catalyst. In p-Si|Ti|TiO_2|-PDI'-NiCt, the photogenerated electrons at the p-Si conduction band edge are transferred to PDI'* (E(PDI'^*/PDI'^{*-}) ~ 1.61 V vs NHE [29]) to give the anion PDI'^- for catalyst reduction, Figure 2d. The involvement of the excited-state and ground-state redox couples of PDI' (PDI'^{*0}/PDI^- and PDI'^0/PDI^-) contributes to the enhanced photocurrents by providing a large driving force (~ 2.3 eV) for efficient electron transfer from the p-Si conduction band to PDI'*.

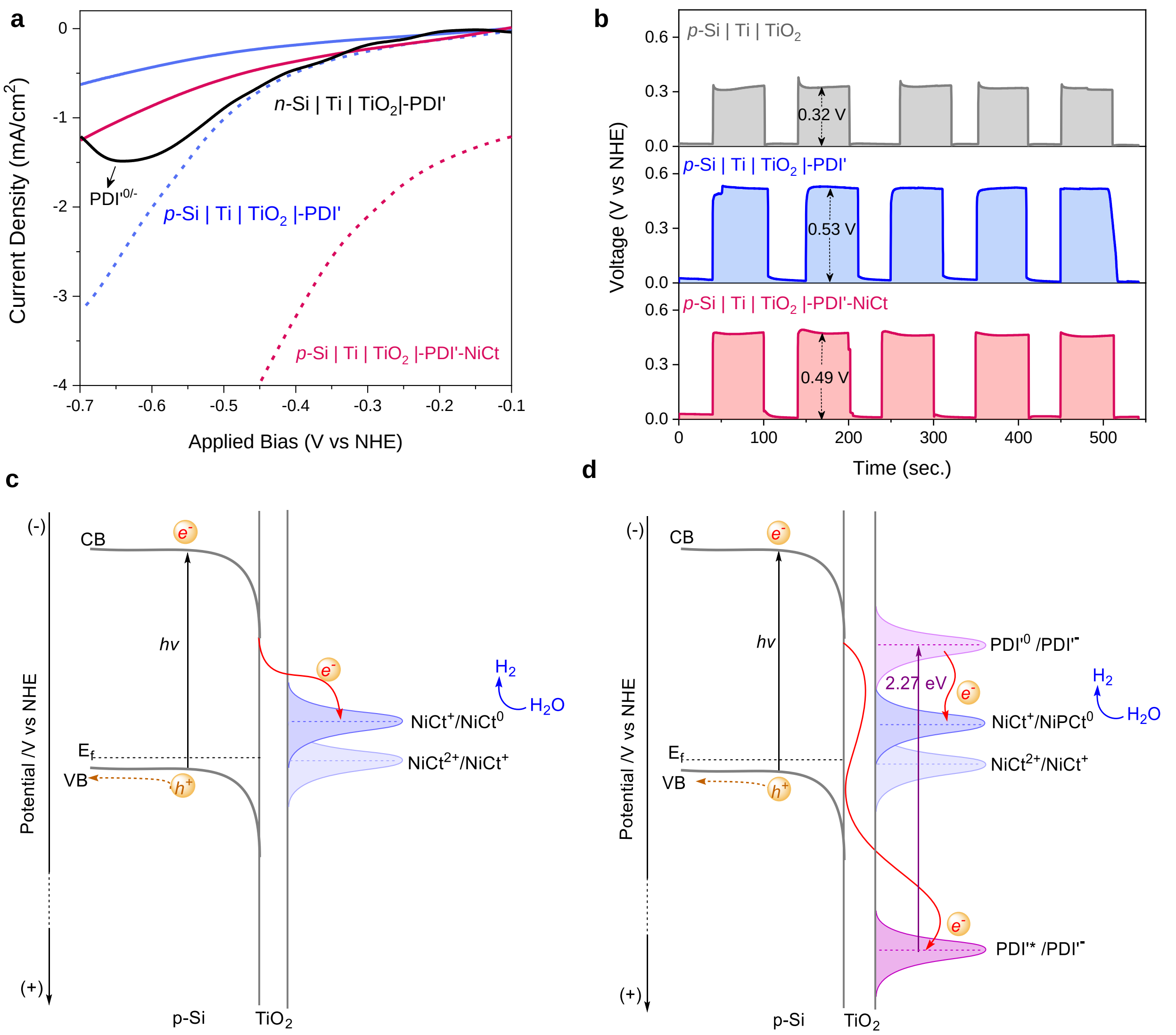

Figure 2. **a**, Linear sweep voltammograms (LSVs) for p-Si|Ti|TiO_2|-PDI’ under dark (solid blue line) or illumination (dashed blue line), n-Si|Ti|TiO_2|-PDI’ under dark (black line), and p-Si|Ti|TiO_2|-PDI’-NiCt under dark (solid red line) or illumination (dashed red line). **b**, Open-circuit voltage (V_{OC}) vs time characteristics for p-Si|Ti|TiO_2 (grey), p-Si|Ti|TiO_2|-PDI’ (blue) and p-Si|Ti|TiO_2|-PDI’-NiCt (red), under chopped light illumination. The light intensity was 100 mW cm^{-2} (AM 1.5G). **c**, **d**, Energy-band diagrams for p-Si|Ti|TiO_2|-NiCt (**c**) and p-Si|Ti|TiO_2|-PDI’-NiCt (**d**), showing the energy alignment between p-Si conduction/valence bands and the redox states of the surface molecules (blue shading for $NiCt^{2+}/NiCt^{+}$ and $NiCt^{+}/NiCt^{0}$; red shading for PDI’*/PDI’$^-$ and PDI’^{0}/PDI’$^-$). All samples were immersed in N_2-degassed, pH 4.5 acetate (0.1 M) buffer with 0.9 M $NaClO_4$ as the supporting electrolyte.

LSVs for the photocathodes under chopped light irradiation in Figure 3a,b further illustrate the role of the electron-mediating PDI’ excited state. Based on the results shown, the photocurrent density for p-Si|Ti|TiO_2|-PDI’-NiCt reaches ~ -1.0 mA/cm^2 under zero bias (vs NHE) and increases rapidly as the bias was decreased further. The photocurrents are also dependent on the electrolyte pH, with data shown in Figure 3c for p-Si|Ti|TiO_2|-PDI’-NiCt in pH 3.0, 4.5 and 5.5 buffers. Compared to pH 4.5, a decrease to pH 3.0 slightly increases the photocurrents under bias more negative than ~ -0.22 V vs NHE. Increasing the pH to 5.5 lowers the photocurrents, presumably because of a decrease in the concentration of protons for protonating the reduced catalyst [41] and the increased energy barrier for H_2 evolution. As expected, the two photocathodes, p-Si|Ti|TiO$_2$|-NiCt and p-Si|Ti|TiO$_2$|-PDI'-NiCt, respond differently to variations in the excitation wavelength. The incident photon-to-current efficiency (IPCE) data are given in Figure 3d. With the PDI' layer, the photocathode p-Si|Ti|TiO$_2$|-PDI'-NiCt shows enhanced IPCE, compared to p-Si|Ti|TiO$_2$|-NiCt, in a wavelength range of ~ 450 nm – 600 nm consistent with the absorption profile of PDI'.

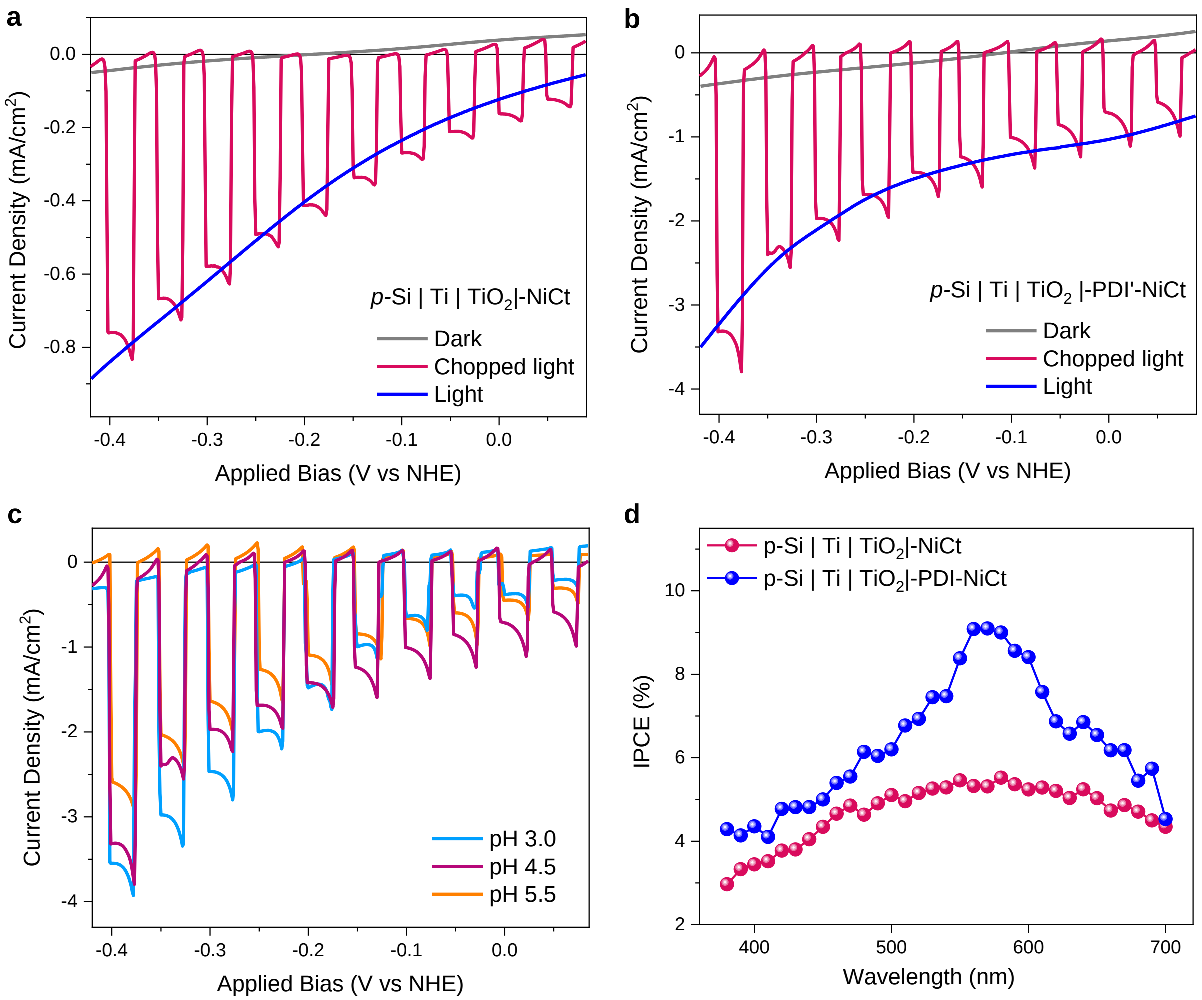

Figure 3. Current densities for p-Si|Ti|TiO$_2$|-NiCt (**a**) and p-Si|Ti|TiO$_2$|-PDI'-NiCt (**b**) under dark (grey), light (blue) or chopped light (red). **c**, Current densities for p-Si|Ti|TiO$_2$|-PDI'-NiCt under chopped light irradiation as a function of pH in the electrolyte with an ionic strength of 1.0 M. **d**, Incident photon-to-current efficiency (IPCE) data for p-Si|Ti|TiO$_2$|-NiCt (red curve) and p-Si|Ti|TiO$_2$|-PDI'-NiCt (blue curve) under an applied bias at -0.15 V versus NHE in pH 4.5 acetate buffer with an ionic strength of 1.0 M.

Based on the photovoltage, the photocathode p-Si|Ti|TiO_2|-PDI'-NiCt upon light irradiation can be coupled with a range of photoanodes in tandem cells for overall solar-driven water splitting. In order to explore the combined photoelectrodes, we have constructed a multi-photon tandem cell with the photoelectrodes in Figure 4. As shown in Figure 5a, the cell consists of the photocathode (Figure 4a) described here and a dye-sensitized photoanode (Figure 4b) based on a nanocrystalline (particle size: ~ 18 nm), core-shell structured n-type semiconductor, SnO_2 (4.5 μm)|TiO_2 (3.0 nm) [42]. For the photoanode, the SnO_2|TiO_2 electrode was surface-modified by stepwise addition of a chromophore [Ru^{II}(4,4'-$(CH_2PO_3H_2)_2$-2,2'-bipyridine$)_2$(2,2′-bipyridine)]Cl_2 (abbreviated as RuP_2^{2+}) and a catalyst Ru(2,2'-bipyridine-6,6'-dicarboxylate)(pyridine-4-butyl-phosphonic acid$)_2$ (abbreviated as RuCt) [36, 43]. The chromophore and catalyst were interconnected by a Zr^{IV}-phosphonate bridge. The performance of the photoanode in a single-junction cell with a Pt dark cathode is shown in Figure S3 with the IPCE data in Figure S4.

For the integrated cell, the surface coverages of the molecular components and their light absorption efficiencies are detailed in Table S1. The chromophore RuP_2^{2+} captures blue light in the incident photons. In constructing the tandem water-splitting cell, placing the photoanode in front of the cell enables absorption and conversion of the higher energy photons for water oxidation. The lower energy photons transmitted by the photoanode are absorbed by the photocathode. Specifically, the transmitted green and red light photons are captured by PDI' and p-Si, respectively, to drive the reduction of NiCt towards H_2 evolution. Figures 5b and S2 show the configuration of the tandem cell with external electrical connection and gas outlets for monitoring the current signals and product quantification.

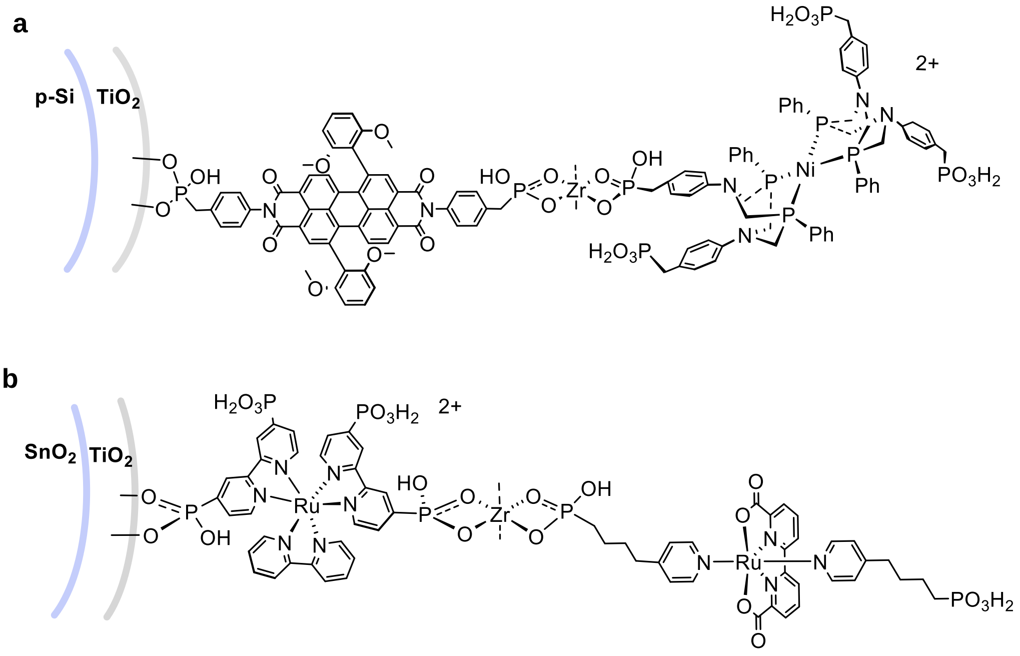

Figure 4. Structures of the photocathode (**a**) and photoanode (**b**) in the tandem PEC.

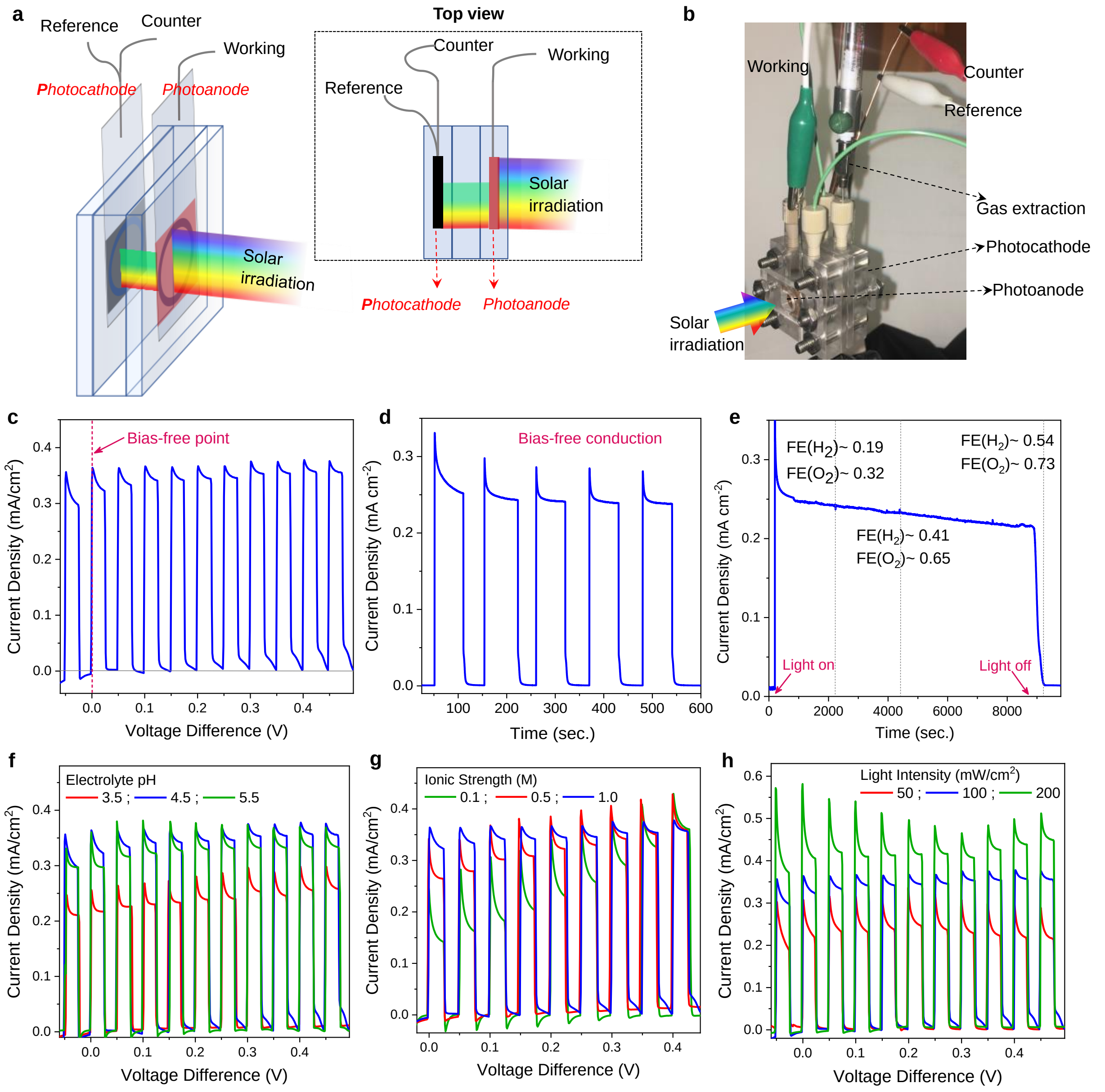

Figure 5. **a**, Side- and top-view of the tandem water-splitting cell with the photocathode (p-Si|Ti|TiO_2|-PDI′-NiCt) and the photoanode (SnO_2|TiO_2|-RuP_2^{2+}-RuCt) in two compartments separated by a proton exchange membrane. **b**, The tandem cell setup during photoelectrocatalytic measurements with the compartments sealed by caps with ports for access to N_2-purging and extraction of gas from the headspace. **c**,**d**, Current-voltage (**c**) and current-time (**d**) curves for the tandem cell under chopped light irradiation. **e**, Long-term photocurrent for the tandem cell. For **c-e**, the electrolyte used was 0.1 M, pH 4.5 acetate buffer with 0.9 M $NaClO_4$ and irradiation intensity was 100 mW cm^{-2}. **f**,**g**,**h**, Current-voltage curves for the tandem cell under chopped light irradiation at various pH (**f**), ionic strengths by changing the concentration of $NaClO_4$ (**g**), and irradiation intensities (**h**). For **f-h**, except the varied conditions in the legends, all other conditions (pH, ionic strength and light intensity) were kept the same as those for **c-e**.

Current-voltage characteristics for the final cell under chopped light irradiation (AM 1.5 G, 100 mW cm^{-2}) are given in Figure 5c. The data show that there are no significant current variations when the applied voltage between the photoanode and the photocathode is varied from 0 V to 0.5 V. Based on the current-time trace in Figure 5d, the tandem cell under zero applied bias yields an initial photocurrent density of ~ 0.3 mA/cm^2 which decreases by ~ 17% within 10 min. In the long-term photocurrent trace in Figure 5e, the photocurrent density drops by ~ 31% during 2 hours of irradiation. The Faradaic efficiencies (FE) for H_2 and O_2 evolution measured at 34 min, 68 min and 138 min are listed in Figure 5e. The overall distributions of FE(H_2) and FE(O_2) are much less than unity, because of the presence of non-catalytic photocurrents for oxidation of dissolved O_2 and trace impurities in the electrolyte solutions. From the results, FE(H_2) increased from 0.19 to 0.54 and FE(O_2) from 0.32 to 0.73 during the first 2 hours of photoelectrocatalysis. The significant initial variations in performance may originate from non-catalytic behaviors before equilibration of catalysis was established. The quantum yield for H_2 production by the tandem cell under zero bias over a two-hour period of irradiation was ~ 0.32% (see details in the Experimental Section) based on the incident photon flux of 2.46×10^{17} photons s^{-1} cm^{-2}.

An important design parameter for a tandem device is the cell-operating pH and ionic strength of the electrolyte. The pH-dependence is illustrated Figure 5f. The low photocurrents at pH 3.5 result from the reduced efficiency of the photoanode (Figure S5) which limits the overall performances. Lowering the pH leads to increased energy barrier and decreased driving force for RuCt activation [43, 44], which in turn reduces the photoanode efficiency. In Figure 5f, increasing the pH to 5.5 does not change the photocurrent significantly. We have demonstrated in Figure 3c that the photoelectrocatalytic performances of the single photocathode decreases noticeably as the pH was increased to 5.5. The photoelectrocatalytic efficiency of the photoanode varies marginally as the pH is increased from 4.5 to 5.5 (Figure S5). The fact that the tandem cell generates similar photocurrents at pH 5.5 and 4.5 further indicates that the photoelectrocatalytic performances are limited by the photoanode.

As shown by the photocurrent results in Figure 5g, decreasing the ionic strength from 1.0 to 0.1 at consistent pH diminishes the cell efficiency. The appearance of ionic strength effect is expected, with ionic strength sufficiently high for minimizing ohmic losses across the cell [4, 10]. At low ionic strengths (0.1 M and 0.5 M), the solution resistance is increased, which in turn causes the operating point to drop to lower operating current densities and decreases the photoelectrocatalytic efficiency.

Besides the electrolyte pH and ionic strength, the irradiation intensity also determines the number of photogenerated redox-separated states and thus controls the overall photoelectrocatalytic performances. In Figure 5h, the photocurrent densities are enhanced or reduced by ~ 29% upon changing the irradiation intensities to 200 mW cm^{-2} or 50 mW cm^{-2}, respectively. Since the number of redox-separated states at the photoanode is controlled by the incident photon flux, a change at the light intensity is directly revealed at the photocurrent densities from the tandem cell.

CONCLUSIONS

A chemically modified, p-Si heterojunction photocathode has been prepared for water reduction to H_2. It was based on TiO_2-protected p-Si nanowire arrays that were surface-modified with a perylene-diimide derivative (PDI'). Following excitation, the PDI' forms a strongly electron-deficient excited state for extraction of photogenerated minority carriers at p-Si*. Coupled with a surface-attached molecular nickel catalyst, the integrated photocathode was capable to deliver a photocurrent density of ~ -1.0 mA/cm^2 under zero applied bias (vs NHE), remarkably outperforming the p-Si|Ti|TiO$_2$ counterpart.

With the results from the single-junction photocathode in hand, experiments were extended to a tandem device which couples the photocathode with an oxide-based, dye-sensitized photoanode for solar-driven water splitting to H_2 and O_2 in separate cell compartments. The tandem cell utilizes the high-energy photons from the incident light to drive water oxidation at the photoanode and the low-energy photons to drive water reduction at the p-Si photocathode. Results from photoelectrocatalytic measurements reveal that the overall cell efficiency is limited by the performance of the photoanode. The results obtained here are significant in pointing to a novel approach based on molecular surface-modification for improving the performances of semiconductor-based photoelectrodes, past current existing Si photoelectrode designs, that could provide a general strategy for water-splitting solar cells.

EXPERIMENTAL SECTION

Synthesis of the photocathodes. The boron-doped p-Si(100) wafer (525 m thick, 1-5 Ω cm) purchased from University Wafers was cut into 1.2 × 1.2 cm^2 squares. The squares were cleaned stepwise by sonicating in acetone, ethanol and water, respectively, for 10 min each, soaking in H_2SO_4 /H_2O_2 /H_2O (volume ratio: 1:1:1) for 30 min, and finally sonicating in HF (aq., 5%) for 10 min. Each cleaned p-Si square was etched in an aqueous mixture of HF (10%, 40 mL) and $AgNO_3$ (136 mg) at 50 °C for 45 min, followed by removal of surface Ag by soaking in concentrated HNO_3 solution (aq., 68.0-70.0%) for 30 min [30-32]. The resulting p-Si nanowire electrodes were then modified by sputtering with a thin Ti layer (~10 nm) via a Kurt Lesker PVD 75 magnetron sputtering system. The p-Si|Ti electrode was deposited with TiO_2 layer (~ 3.0 nm) by atomic layer deposition (ALD) with tetrakis-dimethylamido titanium as the precursor [34].

For the photocathodes, the molecular chromophore (PDI': N,N'-di(4-benzylphosphonic acid)-1,7-di(2,6-dimethoxyphenyl) perylene-3,4,9,10-tetracarboxylic acid bisimide) [29] and catalyst (NiCt: $[[Ni(P_2^{Ph}N_2^{C_6H_4CH_2PO_3H_2})_2]^{2+}$) were synthesized using previously reported procedures [26-28]. The p-Si|Ti|TiO$_2$ electrode was further modified with the chromophore-catalyst assembly by soaking in solutions of PDI' (0.5 mM, in 1:1 DMSO/MeOH), $ZrOCl_2$ (3.0 mM, in MeOH) and NiCt (0.5 mM, in N_2-degassed MeOH), respectively, for 10 hours each. Loading of the catalyst was carried out in a N_2-purged glovebox [28]. The p-Si photocathodes with molecular assemblies were attached to FTO glass by the following method. The back side of p-Si was first cleaned with a HF (5%, aq.)-soaked cotton swab to remove surface SiO_2. Ga−In eutectic (Sigma Aldrich) alloy was then deposited on the back side of p-Si to form an ohmic contact. The back side was subsequently attached to FTO coated glass (1.5 × 4.0 cm^2) using silver epoxy paste. The assembled photocathodes were dried at room temperature in the N_2-purged glovebox for 4 hours before measurements.

Synthesis of the photoanodes. The nanocrystalline SnO_2 substrate was synthesized from a reported method[45, 46]. The SnO_2 film was then modified with a TiO_2 layer (~3.0 nm) by ALD with tetrakis-dimethylamido titanium as the precursor[34]. The molecular components, the RuP_2^{2+} chromophore

($[Ru^{II}(4,4'-(CH_2PO_3H_2)_2$-2,2'-bipyridine$)_2$(2,2′-bipyridine)$]Cl_2$) and the RuCt catalyst (Ru(6,6'-bda)(pyridine-4-butyl-phosphonic acid$)_2$; bda: 2,2'-bipyridine-6,6′-dicarboxylate) were synthesized based on the reported procedures [43, 47, 48]. The $SnO_2|TiO_2$ electrode was further modified with the chromophore-catalyst assembly by soaking in methanol solutions of RuP_2^{2+} (0.5 mM), $ZrOCl_2$ (3.0 mM) and RuCt (0.5 mM), respectively, for 10 hours each. Loading of the RuCt catalyst was carried out in a N_2-purged glovebox[28].

Photoelectrocatalytic measurements. As shown in Figures 5 and S2, the tandem cell contained two compartments for the photocathode and the photoanode which were separated with a proton exchange membrane (Nafion 117). Except for the pH- and ionic strength-dependent experiments, the two compartments were filled with pH 4.5 acetate (0.1 M) buffer with 0.9 M $NaClO_4$ as the supporting electrolyte and sealed with PEEK caps with ports for access for N_2-purging and extraction of gas from the headspace. A CHI 601D potentiostat was used to supply the applied bias for the cells and record the current–time and potential-time signals. Light illumination was provided by an AM1.5 G, 100 mW cm^{-2} solar simulator (NEWPORT 1000-W Xe lamp with an AM1.5 filter) whose light intensity was calibrated with a standard p-Si cell. For the three-electrode photoelectrocatalytic measurements, a custom-made, two-compartment photoelectro-chemical cell was used as reported earlier [28]. A platinum mesh counter electrode and a Ag/AgCl reference electrode were immersed in the electrolyte in one of the compartments.

The water-splitting products, H_2 and O_2, were quantified by gas chromatography equipped with both thermal conductivity detector (TCD) and flame ionization detector (FID) [29]. An aliquot of gas (500 μL) was extracted from the headspace of each electrode compartment and injected into a gas chromatography analyzing system (Varian 450-GC) that was calibrated with a standard gas mixture (H_2, O_2, CH_4, CO and CO_2 in N_2) before the product measurements. The signals of H_2 and O_2 were linearly converted into partial pressures based on Henry's Law for quantification of dissolved H_2 and O_2, which were added to the amount of H_2 and O_2 in the headspace for estimation of overall H_2 and O_2 evolution. Except H_2 and O_2, no other products were detected by GC. The Faradaic efficiencies (FE) of H_2 and O_2 were estimated from eqs. 1 and 2, respectively.

$$FE(H_2) = 2\times\frac{\text{moles of } H_2}{\text{moles of electrons}} \quad \text{eq. 1}$$

$$FE(O_2) = 4\times\frac{\text{moles of } O_2}{\text{moles of electrons}} \quad \text{eq. 2}$$

The values of moles of electrons were from the integrals of the photocurrent curves.

Capacitance measurements. The capacitance measurements were carried out with a Gamry Reference 600 electrochemical impedance spectrometer at a 50 mV voltage step by applying an AC voltage at 50 mV root-mean-square amplitude at a frequency of 1.0 kHz. The three-electrode photoelectrochemical cell was half-filled with N_2-purged pH 4.5 acetate (0.1 M) buffer with 0.9 M $NaClO_4$ as the supporting electrolyte. A platinum mesh and a Ag/AgCl electrode were used as the counter and reference electrodes, respectively.

ASSOCIATED CONTENT

Supporting Information

Synthetic scheme, tandem cell compositions, photoanode structure, additional photocurrent data, additional tables of efficiencies, and ground/excited state potentials.

AUTHOR INFORMATION

Corresponding Author

*tjmeyer@unc.edu

Notes

The authors declare no competing financial interest.

ACKNOWLEDGMENTS

The research on the photoelectrodes and photoelectrocatalysis (at UNC-Chapel Hill) were supported by the U.S. Department of Energy, Office of Science, Office of Basic Energy Sciences, under Award No. DE-SC0015739. The design and synthesis of the nickel-based catalyst (at PNNL) were supported as part of the Center for Molecular Electrocatalysis, an Energy Frontier Research Center funded by the U.S. Department of Energy, Office of Science, Office of Basic Energy Sciences. PNNL is operated by Battelle for the U.S. Department of Energy. The experiments with the solar simulator were performed with the instruments within the AMPED EFRC Instrumentation Facility established by the Alliance for Molecular PhotoElectrode Design for Solar Fuels, an Energy Frontier Research Center funded by the U.S. Department of Energy, Office of Science, Office of Basic Energy Sciences under Award DE-SC0001011. The ALD experiments were performed at the Chapel Hill Analytical and Nanofabrication Laboratory, a member of the North Carolina Research Triangle Nanotechnology Network supported by the National Science Foundation, Grant ECCS-1542015, as part of the National Nanotechnology Coordinated Infrastructure.

REFERENCES

1. Walter, M. G.; Warren, E. L.; McKone, J. R.; Boettcher, S. W.; Mi, Q.; Santori, E. A.; Lewis, N. S., Solar Water Splitting Cells. *Chem. Rev.* **2010,** *110*, 6446-6473.
2. Turner, J.; Sverdrup, G.; Mann, M. K.; Maness, P.-C.; Kroposki, B.; Ghirardi, M.; Evans, R. J.; Blake, D., Renewable hydrogen production. *Int. J. Energy Res.* **2008,** *32*, 379-407.
3. Weber, M. F.; Dignam, M. J., Splitting water with semiconducting photoelectrodes—Efficiency considerations. *Int. J. Hydrog. Energy* **1986,** *11*, 225-232.
4. Hu, S.; Xiang, C.; Haussener, S.; Berger, A. D.; Lewis, N. S., An analysis of the optimal band gaps of light absorbers in integrated tandem photoelectrochemical water-splitting systems. *Energy Environ. Sci.* **2013,** *6*, 2984-2993.
5. Shockley, W.; Queisser, H. J., Detailed Balance Limit of Efficiency of p-n Junction Solar Cells. *J. Appl. Phys.* **1961,** *32*, 510-519.

6. Khaselev, O.; Turner, J. A., A Monolithic Photovoltaic-Photoelectrochemical Device for Hydrogen Production via Water Splitting. *Science* **1998,** *280*, 425.

7. He, J.; Lindström, H.; Hagfeldt, A.; Lindquist, S.-E., Dye-sensitized nanostructured tandem cell-first demonstrated cell with a dye-sensitized photocathode. *Sol. Energy Mater Sol. Cells* **2000,** *62*, 265-273.

8. Tong, L.; Iwase, A.; Nattestad, A.; Bach, U.; Weidelener, M.; Götz, G.; Mishra, A.; Bäuerle, P.; Amal, R.; Wallace, G. G.; Mozer, A. J., Sustained solar hydrogen generation using a dye-sensitised NiO photocathode/BiVO4 tandem photo-electrochemical device. *Energy Environ. Sci.* **2012,** *5*, 9472.

9. Prévot, M. S.; Sivula, K., Photoelectrochemical Tandem Cells for Solar Water Splitting. *J. Phys. Chem. C* **2013,** *117*, 17879-17893.

10. Seger, B.; Castelli, I. E.; Vesborg, P. C. K.; Jacobsen, K. W.; Hansen, O.; Chorkendorff, I., 2-Photon tandem device for water splitting: comparing photocathode first versus photoanode first designs. *Energy Environ. Sci.* **2014,** *7*, 2397-2413.

11. Li, F.; Fan, K.; Xu, B.; Gabrielsson, E.; Daniel, Q.; Li, L.; Sun, L., Organic Dye-Sensitized Tandem Photoelectrochemical Cell for Light Driven Total Water Splitting. *J. Am. Chem. Soc.* **2015,** *137*, 9153-9159.

12. Walczak, K.; Chen, Y.; Karp, C.; Beeman, J. W.; Shaner, M.; Spurgeon, J.; Sharp, I. D.; Amashukeli, X.; West, W.; Jin, J.; Lewis, N. S.; Xiang, C., Modeling, Simulation, and Fabrication of a Fully Integrated, Acid-stable, Scalable Solar-Driven Water-Splitting System. *ChemSusChem* **2015,** *8*, 544-551.

13. Wang, Q.; Hisatomi, T.; Jia, Q.; Tokudome, H.; Zhong, M.; Wang, C.; Pan, Z.; Takata, T.; Nakabayashi, M.; Shibata, N.; Li, Y.; Sharp, I. D.; Kudo, A.; Yamada, T.; Domen, K., Scalable water splitting on particulate photocatalyst sheets with a solar-to-hydrogen energy conversion efficiency exceeding 1%. *Nat. Mater.* **2016,** *15*, 611.

14. Gibson, E. A., Dye-sensitized photocathodes for H_2 evolution. *Chem. Soc. Rev.* **2017,** *46* (20), 6194-6209.

15. Wu, H.-L.; Li, X.-B.; Tung, C.-H.; Wu, L.-Z., Recent Advances in Sensitized Photocathodes: From Molecular Dyes to Semiconducting Quantum Dots. *Adv. Sci.* **2018,** *5*, 1700684.

16. Boettcher, S. W.; Spurgeon, J. M.; Putnam, M. C.; Warren, E. L.; Turner-Evans, D. B.; Kelzenberg, M. D.; Maiolo, J. R.; Atwater, H. A.; Lewis, N. S., Energy-Conversion Properties of Vapor-Liquid-Solid–Grown Silicon Wire-Array Photocathodes. *Science* **2010,** *327*, 185.

17. Kumar, B.; Smieja, J. M.; Kubiak, C. P., Photoreduction of CO_2 on p-type Silicon Using Re(bipy-But)$(CO)_3$Cl: Photovoltages Exceeding 600 mV for the Selective Reduction of CO_2 to CO. *J. Phys. Chem. C* **2010,** *114*, 14220-14223.

18. Boettcher, S. W.; Warren, E. L.; Putnam, M. C.; Santori, E. A.; Turner-Evans, D.; Kelzenberg, M. D.; Walter, M. G.; McKone, J. R.; Brunschwig, B. S.; Atwater, H. A.; Lewis, N. S., Photoelectrochemical Hydrogen Evolution Using Si Microwire Arrays. *J. Am. Chem. Soc.* **2011,** *133*, 1216-1219.

19. Hou, Y.; Abrams, B. L.; Vesborg, P. C. K.; Björketun, M. E.; Herbst, K.; Bech, L.; Setti, A. M.; Damsgaard, C. D.; Pedersen, T.; Hansen, O.; Rossmeisl, J.; Dahl, S.; Nørskov, J. K.; Chorkendorff, I., Bioinspired molecular co-catalysts bonded to a silicon photocathode for solar hydrogen evolution. *Nat. Mater.* **2011,** *10*, 434.

20. Sun, K.; Shen, S.; Liang, Y.; Burrows, P. E.; Mao, S. S.; Wang, D., Enabling Silicon for Solar-Fuel Production. *Chem. Rev.* **2014,** *114*, 8662-8719.

21. Ji, L.; McDaniel, M. D.; Wang, S.; Posadas, A. B.; Li, X.; Huang, H.; Lee, J. C.; Demkov, A. A.; Bard, A. J.; Ekerdt, J. G.; Yu, E. T., A silicon-based photocathode for water reduction with an epitaxial SrTiO3 protection layer and a nanostructured catalyst. *Nat. Nanotechnol.* **2014,** *10*, 84.

22. Benck Jesse, D.; Lee Sang, C.; Fong Kara, D.; Kibsgaard, J.; Sinclair, R.; Jaramillo Thomas, F., Designing Active and Stable Silicon Photocathodes for Solar Hydrogen Production Using Molybdenum Sulfide Nanomaterials. *Adv. Energy Mater.* **2014,** *4*, 1400739.

23. Leung, J. J.; Warnan, J.; Nam, D. H.; Zhang, J. Z.; Willkomm, J.; Reisner, E., Photoelectrocatalytic H2 evolution in water with molecular catalysts immobilised on p-Si via a stabilising mesoporous TiO2 interlayer. *Chem. Sci.* **2017,** *8*, 5172-5180.

24. Bookbinder, D. C.; Bruce, J. A.; Dominey, R. N.; Lewis, N. S.; Wrighton, M. S., Synthesis and characterization of a photosensitive interface for hydrogen generation: Chemically modified p-type semiconducting silicon photocathodes. *Proc. Natl. Acad. Sci. U.S.A.* **1980,** *77*, 6280.

25. Dominey, R. N.; Lewis, N. S.; Bruce, J. A.; Bookbinder, D. C.; Wrighton, M. S., Improvement of photoelectrochemical hydrogen generation by surface modification of p-type silicon semiconductor photocathodes. *J. Am. Chem. Soc.* **1982,** *104*, 467-482.

26. Kilgore, U. J.; Roberts, J. A. S.; Pool, D. H.; Appel, A. M.; Stewart, M. P.; DuBois, M. R.; Dougherty, W. G.; Kassel, W. S.; Bullock, R. M.; DuBois, D. L., $[\mathrm{Ni}(\mathrm{P}^{\mathrm{Ph}}{}_{2}\mathrm{N}_{\mathrm{C6H4X2}})_{2}]^{2+}$ Complexes as Electrocatalysts for H_2 Production: Effect of Substituents, Acids, and Water on Catalytic Rates. *J. Am. Chem. Soc.* **2011,** *133*, 5861-5872.

27. Gross, M. A.; Creissen, C. E.; Orchard, K. L.; Reisner, E., Photoelectrochemical hydrogen production in water using a layer-by-layer assembly of a Ru dye and Ni catalyst on NiO. *Chem. Sci.* **2016,** *7*, 5537-5546.

28. Shan, B.; Das, A. K.; Marquard, S.; Farnum, B. H.; Wang, D.; Bullock, R. M.; Meyer, T. J., Photogeneration of hydrogen from water by a robust dye-sensitized photocathode. *Energy Environ. Sci.* **2016,** *9*, 3693-3697.

29. Shan, B.; Nayak, A.; Brennaman, M. K.; Liu, M.; Marquard, S. L.; Eberhart, M. S.; Meyer, T. J., Controlling Vertical and Lateral Electron Migration Using a Bifunctional Chromophore Assembly in Dye-Sensitized Photoelectrosynthesis Cells. *J. Am. Chem. Soc.* **2018,** *140*, 6493-6500.

30. Peng, K. Q.; Yan, Y. J.; Gao, S. P.; Zhu, J., Synthesis of Large-Area Silicon Nanowire Arrays via Self-Assembling Nanoelectrochemistry. *Adv. Mater.* **2002,** *14*, 1164-1167.

31. Yu, H.; Li, X.; Quan, X.; Chen, S.; Zhang, Y., Effective Utilization of Visible Light (Including $\lambda > 600$ nm) in Phenol Degradation with p-Silicon Nanowire/TiO_2 Core/Shell Heterojunction Array Cathode. *Environ. Sci. Technol.* **2009,** *43*, 7849-7855.

32. Torralba-Peñalver, E.; Luo, Y.; Compain, J.-D.; Chardon-Noblat, S.; Fabre, B., Selective Catalytic Electroreduction of CO2 at Silicon Nanowires (SiNWs) Photocathodes Using Non-Noble Metal-Based Manganese Carbonyl Bipyridyl Molecular Catalysts in Solution and Grafted onto SiNWs. *ACS Catal.* **2015,** *5*, 6138-6147.

33. Bae, D.; Seger, B.; Vesborg, P. C. K.; Hansen, O.; Chorkendorff, I., Strategies for stable water splitting via protected photoelectrodes. *Chem. Soc. Rev.* **2017,** *46*, 1933-1954.

34. Alibabaei, L.; Brennaman, M. K.; Norris, M. R.; Kalanyan, B.; Song, W.; Losego, M. D.; Concepcion, J. J.; Binstead, R. A.; Parsons, G. N.; Meyer, T. J., Solar water splitting in a molecular photoelectrochemical cell. *Proc. Natl. Acad. Sci. U.S.A.* **2013,** *110*, 20008-20013.

35. Hanson, K.; Torelli, D. A.; Vannucci, A. K.; Brennaman, M. K.; Luo, H.; Alibabaei, L.; Song, W.; Ashford, D. L.; Norris, M. R.; Glasson, C. R. K.; Concepcion, J. J.; Meyer, T. J., Self-Assembled Bilayer Films of Ruthenium(II)/Polypyridyl Complexes through Layer-by-Layer Deposition on Nanostructured Metal Oxides. *Angew. Chem., Int. Ed.* **2012,** *51*, 12782-12785.

36. Farnum, B. H.; Wee, K.-R.; Meyer, T. J., Self-assembled molecular p/n junctions for applications in dye-sensitized solar energy conversion. *Nat. Chem.* **2016,** *8*, 845-852.

37. Turner, J. A.; Manassen, J.; Nozik, A. J., Photoelectrochemistry with p-Si electrodes: Effects of inversion. *Appl. Phys. Lett.* **1980,** *37*, 488-491.

38. Esposito, D. V.; Levin, I.; Moffat, T. P.; Talin, A. A., H_2 evolution at Si-based metal–insulator–semiconductor photoelectrodes enhanced by inversion channel charge collection and H spillover. *Nat. Mater.* **2013,** *12*, 562.

39. Abruna, H. D.; Bard, A. J., Semiconductor electrodes. 40. Photoassisted hydrogen evolution at poly(benzyl viologen)-coated p-type silicon electrodes. *J. Am. Chem. Soc.* **1981,** *103*, 6898-6901.

40. Yang, Y.; Ciampi, S.; Choudhury, M. H.; Gooding, J. J., Light Activated Electrochemistry: Light Intensity and pH Dependence on Electrochemical Performance of Anthraquinone Derivatized Silicon. *J. Phys. Chem. C* **2016,** *120*, 2874-2882.

41. O'Hagan, M.; Ho, M.-H.; Yang, J. Y.; Appel, A. M.; DuBois, M. R.; Raugei, S.; Shaw, W. J.; DuBois, D. L.; Bullock, R. M., Proton Delivery and Removal in $[Ni(P^{R}_{2}N^{R'}_{2})_{2}]^{2+}$ Hydrogen Production and Oxidation Catalysts. *J. Am. Chem. Soc.* **2012,** *134*, 19409-19424.

42. Alibabaei, L.; Sherman, B. D.; Norris, M. R.; Brennaman, M. K.; Meyer, T. J., Visible photoelectrochemical water splitting into H_2 and O_2 in a dye-sensitized photoelectrosynthesis cell. *Proc. Natl. Acad. Sci. U.S.A.* **2015,** *112* (19), 5899-5902.

43. Duan, L.; Bozoglian, F.; Mandal, S.; Stewart, B.; Privalov, T.; Llobet, A.; Sun, L., A molecular ruthenium catalyst with water-oxidation activity comparable to that of photosystem II. *Nat. Chem.* **2012,** *4*, 418.

44. Duan, L.; Wang, L.; Inge, A. K.; Fischer, A.; Zou, X.; Sun, L., Insights into Ru-Based Molecular Water Oxidation Catalysts: Electronic and Noncovalent-Interaction Effects on Their Catalytic Activities. *Inorg. Chem.* **2013,** *52*, 7844-7852.

45. Chappel, S.; Zaban, A., Nanoporous SnO_2 electrodes for dye-sensitized solar cells: improved cell performance by the synthesis of 18nm SnO_2 colloids. *Sol. Energy Mater Sol. Cells* **2002,** *71*, 141-152.

46. Lee, S.-H. A.; Abrams, N. M.; Hoertz, P. G.; Barber, G. D.; Halaoui, L. I.; Mallouk, T. E., Coupling of Titania Inverse Opals to Nanocrystalline Titania Layers in Dye-Sensitized Solar Cells. *J. Phys. Chem. B* **2008,** *112*, 14415-14421.

47. Norris, M. R.; Concepcion, J. J.; Glasson, C. R. K.; Fang, Z.; Lapides, A. M.; Ashford, D. L.; Templeton, J. L.; Meyer, T. J., Synthesis of Phosphonic Acid Derivatized Bipyridine Ligands and Their Ruthenium Complexes. *Inorg. Chem.* **2013,** *52*, 12492-12501.

48. Wang, D.; Marquard, S. L.; Troian-Gautier, L.; Sheridan, M. V.; Sherman, B. D.; Wang, Y.; Eberhart, M. S.; Farnum, B. H.; Dares, C. J.; Meyer, T. J., Interfacial Deposition of Ru(II) Bipyridine-Dicarboxylate Complexes by Ligand Substitution for Applications in Water Oxidation Catalysis. *J. Am. Chem. Soc.* **2018,** *140*, 719-726.